Monitoring of composite structures using a network of integrated PVDF film transducers

2015 Smart Mater. Struct. 24 055017

(http://iopscience.iop.org/0964-1726/24/5/055017)

IOP Publishing Smart Materials and Structures
Smart Mater. Struct. **24** (2015) 055017 (13pp) doi:10.1088/0964-1726/24/5/055017

Monitoring of composite structures using a network of integrated PVDF film transducers

Enrique Guzmán, Joël Cugnoni and Thomas Gmür

Faculté des Sciences et Techniques de l'Ingénieur (STI), Ecole Polytechnique Fédérale de Lausanne, Station 9, CH-1015 Lausanne, Switzerland

E-mail: thomas.gmuer@epfl.ch

Received 9 September 2014, revised 27 February 2015
Accepted for publication 3 March 2015
Published 16 April 2015

Abstract

Aiming to reduce costs, polyvinylidene difluoride (PVDF) film patches are an emerging alternative to more classic piezoelectric technologies, like ceramic patches, as transducers to measure local deformation in many structural applications. This choice is supported by advantages such as the low weight and mechanical flexibility of PVDF, making this polymer suitable for embedding inside full scale polymer based composite structures. Piezoelectric transducer patches can be used as actuators to dynamically excite full-scale composite structures, and as sensors to measure the strain. The main objective of this paper is to verify that the PVDF transducers can provide exploitable signals in the context of structural health monitoring. In order to do so, two aspects of the design of transducer network are investigated: the optimization of the sensor network, for which the effective independence method is proposed, and the use of operational modal analysis (OMA), since it is a simple method to extract the natural frequencies of a structure from a time series. The results of the analysis are compared to a reference set issued from experimental modal analysis (EMA), a simple, well-known, classic method, which is carried out using accelerometers and an impact hammer. By statistical means, it is shown that there is no significant difference between the two methods, and an optimized PVDF transducer network combined with OMA can perform the dynamic analysis of a structure as well as a classic EMA setup would do. This leads the way to the use of low-cost PVDF embedded transducer networks for robust composite material characterization.

Keywords: operational modal analysis, PVDF film transducers, structural health monitoring, optimal sensor placement

(Some figures may appear in colour only in the online journal)

1. Introduction

Structural health monitoring (SHM) is a currently studied field of research in structural mechanics, and SHM systems have thus emerged during recent years as an interesting alternative option to more classic non-destructive testing techniques in aerospace. This is a new approach since the start of massive use of polymer-based composite materials, belonging to the family of ultra-light structural materials, in the manufacturing of aircraft parts. Even though they present exceptionally high mechanical performance, polymer-based composite materials are more vulnerable than metallic alloys to natural environmental ageing factors such as impacts, heat, cold, chemical corrosive atmosphere, moisture and solar radiation. Thus, special care must be taken when employing composite materials to manufacture airframe components in a full-scale structure. Potential improvements in the continuous health monitoring techniques are constantly being investigated. The development of a SHM system based on reliable, non-destructive and robust monitoring methods, capable of detecting the presence of damage or natural ageing, hence becomes an essential step in the increase of operational safety inside large composite structures.

In a SHM process, the response to the monitoring question goes through a 4-step solution [1–3]: (1) operational evaluation, (2) data acquisition and cleansing, (3) feature extraction and data compression, and (4) statistical model development and evaluation. The solution of the SHM

paradigm involves then the selection of a method, the hardware for data acquisition and the establishment of statistical models for the material ageing or damage. In the current state of the art, many standard surveillance methods are based on modal testing techniques, the best known being perhaps experimental modal analysis (EMA) [4].

Concerning the hardware, new technologies like optical fibre Bragg gratings [5–7], wireless technology [8, 9], semiconductor piezoresistive transducers [10, 11], piezoelectric transducers [12–14] as well as classical hardware like strain gauges and accelerometers are used. These modern technologies carry their own package of advantages and drawbacks, in particular from the economic and the safety points of view.

Crystals (quartz, tourmaline, etc) and ceramics (lead zirconate titanate PZT and other lead molecules, niobates, titanates) are among the most common piezoelectric materials, which are expensive, fragile and not mechanically compliant, therefore not suitable nor adapted for a SHM application. The alternative studied in this paper is the use of polyvinylidene difluoride (PVDF) piezoelectric patch transducers, because of their compliance for *in situ* monitoring due to their low cost of implementation (economic benefits), flexibility and low weight (operational benefits). The survivability of PVDF mechanical and electromechanical properties to artificial ageing protocols has been demonstrated previously [15]. On the other hand, special caution needs to be taken in order to ensure their survival to extreme conditions in case of demanding applications [15]. For all these reasons, the idea of an integrated transducer network is now seen as an interesting solution for PVDF based SHM. To be applicable *in situ*, it is necessary to use a robust sensing method. A dynamic method such as operational modal analysis (OMA) is proposed in this paper. With respect to the classic EMA, OMA has the particularity to assume the randomness of the excitation signal, making necessary to measure only the output signals. As shown by several authors [16–18], these PVDF transducers, despite their relatively low stiffness and block force, can be used as actuators when correctly integrated to a composite structure. This fact leads to a whole new perspective: the OMA of a full-scale structure can be eventually completely carried out by a simple and cheap integrated PVDF transducers network.

The application of OMA to a structural problem raises the question of optimal transducer placement. In the frame of optimal spatial placement, some methods are available in the scientific literature [19–21], but none of them is directly applicable to the case of strain sensors networks. A simple and quick adaptation can nonetheless be considered for the method of the effective independence (EI) by Li *et al* [21], which is based on the notion of controllability and observability of the vibrational system. Based on the proposals by Yam *et al* [22] and Foss [23], a mathematical conversion to pass from 'displacement modes' to 'strain modes' sets the grounds up to use the latter as valid mode shapes.

The objective is then to verify experimentally that PVDF patch transducers, with the proper manufacturing, handling and integration, are capable of providing exploitable electric signals, in order to extract information about the natural frequencies, and thereby about the state of the constitutive properties of a composite panel. The transducer network is expected to be capable of carrying out a signal acquisition (as a sensor) as well as of providing a random excitation (as an actuator) in case the external natural excitation is not sufficient over the analysed frequency band.

2. Approach of the problem

The problem to be solved is the extraction of natural frequencies only from the time signals provided by an integrated transducers network. In the frame of the development of a SHM tool system, the proposed solution to this problem includes the following elements.

(i) The integration of a network of PVDF transducers, which is possible due to the low implementation cost of PVDF patches, and allows increasing the sensitivity, the mode decoupling, reducing the expenses, improving the safety and speeding up the manufacturing process.
(i) The use of OMA, a non-destructive, dynamic, robust method, that only uses the signals provided by the sensor network to assess the structure's state. The excitation can be eventually supplied by a natural exciter (wind, water stream, road, earthquake) or an artificial one (a complementary transducer network acting mechanically on the structure), or a combination of both.

Both points taken into account, the main contribution of this paper is to show experimentally that both OMA and EI can be combined as part of a structural monitoring system that includes an optimally designed PVDF transducer network. Another approached aspect is the robustness of the method with respect to the quality of the excitation source. Since the theoretical formulation developed by OMA authors [21, 24] assumes a white noise excitation, it would be interesting to check how the method works out when this assumption is not strictly required any more. Furthermore, and this is one of the most interesting contributions of this work, the capacity to compensate for a bad structural excitation by transducer actuation is demonstrated as well. This is a strong point highlight, since it shows the worthiness of the method and opens completely new possibilities for the future on modal analysis.

3. Materials and methods

3.1. PVDF film technology

PVDF is a polymer that has been used until now mainly as a surface protective agent, although since the discovery of its remarkable piezoelectric properties, it is increasingly used in sensing and measuring applications.

The PVDF film transducers used through this paper in the experimental protocols are DT1–052 K piezo film patches, supplied by Measurement Specialties Deutschland©

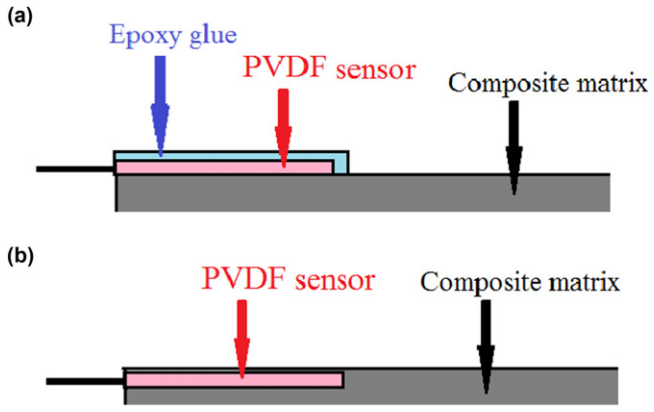

Figure 1. Schemes of sensor mounting: (a) glued PVDF sensor and (b) embedded PVDF sensor.

Table 1. Physical properties of the PVDF film as provided by Measurement Specialties© datasheet.

Thickness (μm)	Young's modulus (GPa)	Piezo strain constant (pC N^{-1})	
t	E	d_{31}	d_{33}
52	3.8	23	−33

(Dortmund, Germany). The physical properties of the PVDF film are summarized in table 1. Each transducer is a 16 mm × 4 mm rectangular flat piece, a similar shape that PZT piezoelectric patches are commonly available in. Mechanically, PVDF transducers have the advantage of compliance, allowing integration in curved areas. The transducers can be either fully integrated on the surface or inside the composite plate between two layers, as shown in figure 1. It has been demonstrated that PVDF transducers are able to survive severe ageing without seeing their dynamic measurement capabilities affected [15]. Concerning the electric signal received from the PVDF sensors, a unit of the multi-channel conditioning amplifier Brüel and Kjæ r 2692-C was used to amplify the time signal from the PVDF transducers, with an equivalent sensitivity adjusted to 101 [pC/V]. On the other hand, as actuators, the commanding electric signals to PVDF transducers are amplified by a SQV 1/500 Analog Amplifier, supplied by Piezomechanik GmbH ® (Munich, Germany). The output signal is adjusted to a fixed gain equal to 100 (V_{peak}= 500 [V]; PVDF transducers can stand 750 [V] so there is no risk).

3.2. Composite specimens and sensor integration

The specimens studied for experimentation are made of Carbon-PrePreg PR-UD CST 125/300 FT109, a carbon fibre/epoxy prepreg composite supplied by Suter-Kunststoffe AG (Switzerland). The raw material is in the form of a unidirectional (UD) carbon tissue (Torayca© T700S carbon fibre), pre-impregnated with slightly cured epoxy polymer (PREDO© FT109) with an areal weight of 125 g m^{-2} (60% of fibre volume fraction). The nominal elastic properties of this material after curing are shown in table 2. The plates were manufactured in autoclave (curing at 85 [°C] and under 5 [bar] for 10 hours, followed by curing at 90 °C and under 5 bar for 4 h). The composite layup was purely UD, with the carbon fibres in the longitudinal direction (see figure 2). The geometrical dimensions and corresponding masses of the plates are summarized in table 3 and were measured using an electronic Vernier and Mettler Toledo© weigh balances respectively (a 0.01 g resolution for the D-series, a 0.1 g resolution for all the others) [25].

3.3. Finite element (FE) model and structural identification algorithm

In SHM, a model is required to relate the measured eigenfrequencies changes to alterations of the constitutive properties. A common first approach to solve the eigenfrequency problem is the use of an FE model, which provides close approximations for the natural frequencies when the dynamic behaviour of specimens is simulated. This FE model was used to build a mixed numerical-experimental identification algorithm, based upon a nonlinear least squares method combined to ABAQUS© FE simulations in order to minimize the error between estimated and experimental frequencies, and to find the most probable values for the elastic properties. A structured mesh with C3D20R quadratic hexahedral elements was generated (in ABAQUS©) for each specimen type, with 2 elements along the thickness. The stiffness matrix is computed using the reduced integration technique.

The specimens were modelled assuming homogeneous orthotropic elastic properties, for which the dynamic properties are determined when nine engineering constants and the density are known. However, depending on the geometry, some of these constants are far more influential than the others. For our specimens, since the thickness-to-length (h/l) and the thickness-to-width (h/w) ratii are very small, these influential constants are expected to be E_1 (longitudinal Young's modulus), E_2 (transversal Young's modulus) and G_{12} (transversal shear modulus). A sensitivity study based on an FE model was performed on the lowest frequency modes to highlight the dominant parameters, as it can be visually verified with figure 3 [25]. The sensitivity parameter is defined as:

$$S = \frac{\Delta f/f}{\Delta E/E}, \tag{1}$$

where S denotes a normalized derivative of the frequency f with respect to the elastic parameter E. For example, in figure 3, it can be seen that the basic vibration modes (flexural and torsional modes) depend essentially on two tensile moduli (E_1 and E_2) and one shear modulus (G_{12}). Experimentally, a low number of measured natural frequencies is then necessary to obtain the basic information to simulate the dynamic behaviour of a sample. In our case, the first eight modes are taken into account, with the corresponding mode shapes.

Table 2. Nominal elastic properties after layup and curing (1: longitudinal direction, 2: transverse direction, 3: normal direction). Over 63 measurements, μ is the average value and σ is the corresponding standard deviation.

	Young's modulus (GPa)			Poisson's ratio (–)			Shear modulus (GPa)		
	E_1	E_2	E_3	ν_{12}	ν_{13}	ν_{23}	G_{12}	G_{13}	G_{23}
μ	96.00	7.67	8.70[a]	0.38[a]	0.3[a]	0.03[a]	3.60	3.59[a]	2.24
σ	0.067	0.013	—	—	—	—	0.021	—	—

[a] Nominal values as supplied in the data sheet.

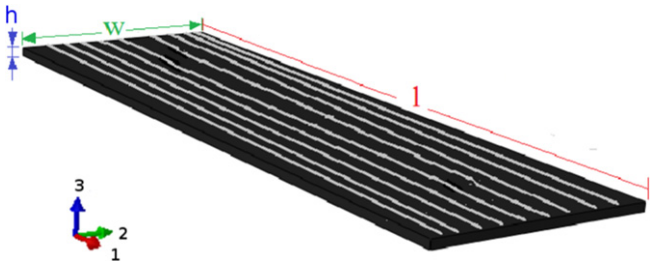

Figure 2. Fibre orientation: 1 = longitudinal direction (length l), 2 = transverse direction (width w), 3 = normal direction (thickness h). Carbon fibres are oriented along 1.

Table 3. Specimen dimensions l, w, h, initial mass m and number of integrated PVDF sensors N.

Sample	l (mm)	w (mm)	h (mm)	m (g)	N (–)
A	300	10.0	4.4	182	3
B	300	9.9	4.6	162	3
C	300	9.9	4.5	181	6
D	300	9.8	4.6	170	6

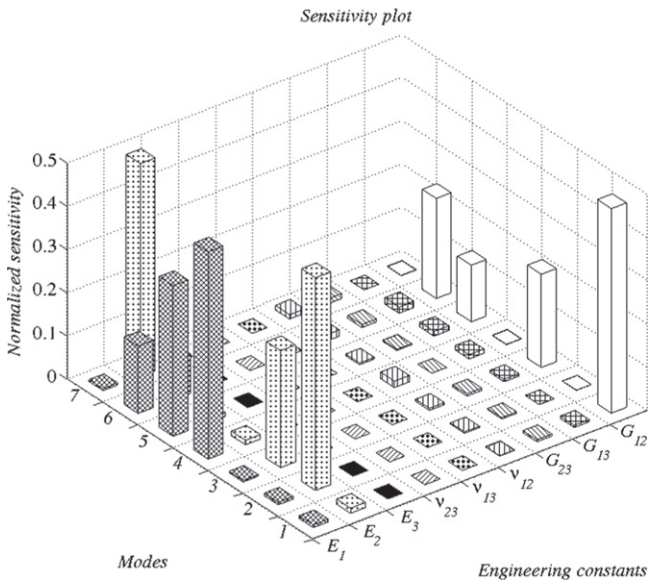

Figure 3. Example of sensitivity analysis between engineering constants and natural frequencies (sample A).

3.4. OMA: a robust monitoring method

Similarly to EMA with the frequency response function (FRF), OMA uses the notion of power spectral density (PSD) to extract the modal parameters of a dynamic system. The fundamental difference is the absence of knowledge about the excitation signal $x(t)$. For the transducer network, the integrated PVDF patches have been used to acquire multiple signals in order to set up a PSD matrix, which is necessary to the extraction of the structural resonance frequencies (and the corresponding mode shapes) of the specimen.

Let us consider the discrete Fourier transform $X_d(\omega)$ of the signal $x(t)$, with a PSD defined as

$$G_{xx}(\omega_k) = (\Delta t)^2 X_d(\omega_k) X_d^*(\omega_k), \tag{2}$$

where Δt is the sampling time and ω_k denotes the k^{th} frequency line. The working hypothesis over $x(t)$ is to assume it as a white noise. By definition, white noise is statistically uncorrelated to itself. This means that $G_{xx}(\omega)$ should be constant for the given frequency band.

Let us consider a multivariate input signal. In this case, a function similar to PSD can be defined:

$$G_{x_i x_j}(\omega_k) = (\Delta t)^2 X_{d_i}(\omega_k) X_{d_j}^*(\omega_k). \tag{3}$$

$G_{x_i x_j}$ is a cross spectral density (CSD) function, for the input signals $x_i(t)$ and $x_j(t)$ (excitation signal at locations i and j). If $\mathbf{H}(\omega_k)$ is the matrix of EMA FRF, a similar PSD matrix for the output signals can be computed [21]:

$$\mathbf{G}_{yy}(\omega_k) = \mathbf{H}^*(\omega_k)\mathbf{G}_{xx}(\omega_k)\mathbf{H}(\omega_k) \tag{4}$$

where $\mathbf{G}_{yy}(\omega_k)$ is the output PSD, $\mathbf{H}(\omega_k)$ is the FRF matrix (the * denotes the corresponding hermitian matrix), and $\mathbf{G}_{xx}(\omega_k)$ is the PSD matrix of the input signals ($[\mathbf{G}_{xx}]_{ij} = G_{x_i x_j}$). In the particular case of OMA, $\mathbf{G}_{xx}(\omega_k) = \mathbf{D}$ becomes a diagonal matrix because of the nature of $x(t)$ (white noise). The PSD matrix $\mathbf{G}_{yy}$ carries all the necessary information about the modal parameters of the structure. The single value decomposition (SVD) is a mathematical tool that can be be applied to $\mathbf{G}_{yy}$ in this case, given its symmetry:

$$\mathbf{G}_{yy}(\omega_k) = \mathbf{U}^*(\omega_k)\mathbf{S}_+(\omega_k)\mathbf{U}(\omega_k), \tag{5}$$

where $\mathbf{S}_+$ is the diagonal matrix of singular values, and the orthogonal matrix $\mathbf{U}$ contains the mode shapes. If done

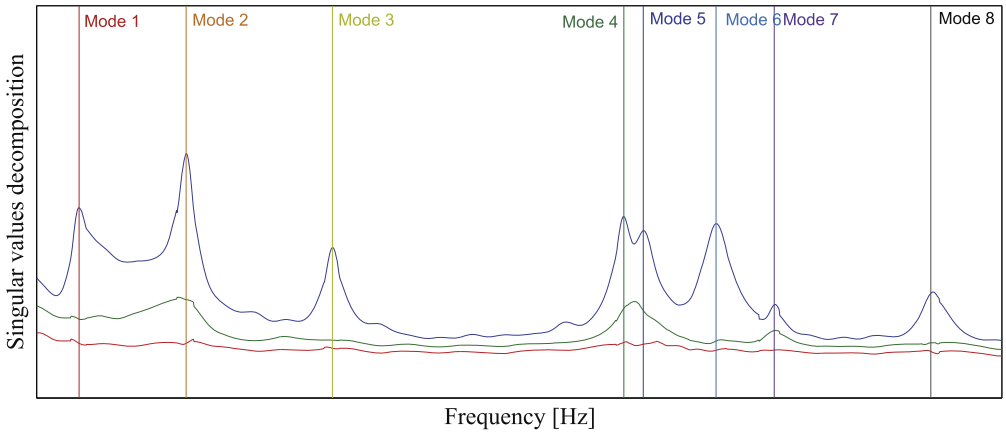

Figure 4. Example of diagonal spectra from a $\mathbf{S}_+$ resulting of a SVD. The vertical lines are the values of the specimen's natural frequencies obtained by EMA.

properly, the SVD gives a diagonal matrix with the diagonal functions ordered in a decreasing order (see figure 4). As can be seen, the natural frequencies are associated to the existence of 'resonance' peaks, as for EMA. Those can be identified by a simple computation using the FSDD method as detailed in [24], which is a third generation frequency-domain decomposition modal extraction method that uses the previous knowledge of a numerical simulated $\mathbf{U}_{\mathrm{FE}}$ from the FE model. This is the method used to determine the natural frequencies of the specimens, as measured by OMA.

Mathematically, FSDD takes the modal assurance criterion (MAC) between the numerically simulated column vectors of $\mathbf{U}_{\mathrm{FE}}$, $\bar{u}_{\mathrm{FE}}$, and the experimentally obtained (by SVD) $\bar{u}$ to define an 'influence zone', in the sense of the single degree of freedom hypothesis: in this zone, it can be assumed that $\mathbf{G}_{yy}$ is dominated by one local mode. The influence zone is defined by the points satisfying the following condition:

$$\mathrm{MAC}(\bar{u}, \bar{u}_{\mathrm{FE}}) = \frac{\bar{u}^{\mathrm{T}}\bar{u}_{\mathrm{FE}}}{|\bar{u}||\bar{u}_{\mathrm{FE}}|} > \mathrm{MAC}_{\mathrm{crit}}. \tag{6}$$

The threshold value $\mathrm{MAC}_{\mathrm{crit}}$ is usually taken above 0.9 for fairly discernible modes, although it should be adapted to higher values if the modal density increases (0.95 in this paper, due to the closeness of the 4th, 5th and 6th modes). Finally, a curve fitting using a polynomial approximation is carried out to extract the local natural frequency.

4. Transducer placement strategy

4.1. EI method

The more complex is the shape, the more sensors placed in strategic places are needed to ensure the observation of all lowest frequency modes. As a general rule, the minimum number of transducers needed to observe/control the vibrational behaviour of a structure depends on the sought modes and their shape. For the dynamic model of a given structure, OMA identifies the modal parameters: natural frequencies, damping factors and deformation modes. In order to identify correctly the natural frequency ω_k of the kth order and the corresponding modal vector $\boldsymbol{\Phi}_k$, the sensors must be located in the right regions. The usefulness of an FE model to determine the couples (ω_k $\boldsymbol{\Phi}_k$) is evident, because an optimal placement can be determined before the manufacturing of the part (with the integrated transducers).

A simple but naive way to place the transducers in the structure is to check visually the distribution of the strain field for each mode, obtained by a numerical modal analysis after of the FE model, and to place the transducers in the regions showing the maximal strain. However, this technique becomes complex and time-consuming when more complex shapes are to be modelled. Smarter and more sophisticated techniques have been developed over the years, as reviewed by Meo *et al* [26]. These techniques are either energy-based or data amount-based. Among the former, the EI technique was validated [27] for aerospace structures and compared to another similar method, called the modal kinetic energy (MKE) method [21]. The EI technique was used by the authors to find the optimal placement described in this paper. An in-house software applying the mathematical principle behind EI was developed using MATLAB©. Both MKE method or EI method can be used to maximize the 'kinetic' energy received by a given number of sensors. An index vector $\boldsymbol{\mathcal{K}}$ is defined, alternatively by two formulae:

$$\boldsymbol{\mathcal{K}} = \mathrm{diag}\left(\boldsymbol{\Phi}\boldsymbol{\Phi}^{\mathbf{T}}\right) \tag{7}$$

for the MKE method, and

$$\boldsymbol{\mathcal{K}} = \mathrm{diag}\left(\boldsymbol{\Phi}\boldsymbol{\Phi}^{+}\right) \tag{8}$$

for the EI method. In these expressions, $\boldsymbol{\Phi}^{\mathbf{T}}$ and $\boldsymbol{\Phi}^{+} = [\boldsymbol{\Phi}^{\mathbf{T}}\boldsymbol{\Phi}]^{-1}\boldsymbol{\Phi}^{\mathbf{T}}$ denote the transpose matrix and the pseudo inverse matrix of the orthonormal matrix $\boldsymbol{\Phi}$, which contains the row-vectors corresponding to the eigenmodes $\boldsymbol{\Phi}_k$ to be observed. The diag() operator denotes the vector formed by the diagonal elements of a matrix. Whether the optimization algorithm uses the MKE or the EI index vector, the approach is the same: let us consider a structure with n possible locations, and consequently n degrees of freedom (DoF) in its

modal representation. After $\mathcal{K}$ is evaluated, the element with the weakest energy (i.e. the lowest value) is tracked. The corresponding row is deleted from $\boldsymbol{\Phi}$ to form a reduced matrix $\boldsymbol{\Phi}_{(1)}$ (with a rank of $n-1$), which is used to evaluate the next iteration $\mathcal{K}_1$ of the index vector, based on formulae (7) and (8) for the MKE and the EI techniques respectively. The procedure is sequentially repeated until the pth iteration, where $p = n - m$: $\mathcal{K}$ has in that case m elements, corresponding to the m optimal regions where the sensors should be placed. The choice of m depends on the needs of the experimenter, although the main criterion is to have a minimum number of transducers with the capability to discern the studied set of eigenmodes [21]. As shown in section 4.3, the placement of $m = 3$ transducers is optimized for the monitoring of 8 eigenmodes.

It has been demonstrated that the two methods are almost equivalent in every point, although the EI technique has the advantage of 'renormalizing' the index vector $\mathcal{K}$ after each iteration. Indeed, when the modal mass matrix $\mathbf{M}$ is not a multiple of the identity matrix $\mathbf{I}$, the index vector for the MKE method is given by:

$$\mathcal{K} = \mathrm{diag}\left(\mathbf{M}^{1/2}\boldsymbol{\Phi}\left[\mathbf{M}^{1/2}\boldsymbol{\Phi}\right]^{\mathbf{T}}\right) \tag{9}$$

and for the EI method by:

$$\begin{aligned}\mathcal{K} &= \mathrm{diag}\left(\mathbf{M}^{1/2}\boldsymbol{\Phi}\left[\left[\mathbf{M}^{1/2}\boldsymbol{\Phi}\right]^{\mathbf{T}}\mathbf{M}^{1/2}\boldsymbol{\Phi}\right]\left[\mathbf{M}^{1/2}\boldsymbol{\Phi}\right]^{\mathbf{T}}\right)\\ &= \mathrm{diag}\left(\boldsymbol{\Phi}\boldsymbol{\Phi}^{+}\right),\end{aligned} \tag{10}$$

where $\mathbf{M}^{1/2}$ is the square root of the symmetric positive modal masses matrix $\mathbf{M}$. It can be seen that $\mathcal{K}$ remains independent of the mass matrix in the case of the EI method.

An inconvenient of this approach is found when n is large, i.e. there are too many DoF, a condition frequently observed when the analysed model is based on the FE formulation. A simplifying additional step is to turn to a triangular-orthogonal QR decomposition in order to speed up the computation. At iteration i, the (reduced) mode shape matrix $\boldsymbol{\Phi}_{(i)} = \mathbf{QR}$ is decomposed, with the unitary orthogonal matrix $\mathbf{Q}_{[n\times p_i]}$ ($p_i = n - i$) and the upper triangular matrix $\mathbf{R}_{[p_i\times p_i]}$ [21]. By substituting $\mathbf{QR}$ in equation (8), the index vector then becomes:

$$\begin{aligned}\mathcal{K} &= \mathrm{diag}\left(\mathbf{QR}\left[\mathbf{R}^{\mathbf{T}}\mathbf{Q}^{\mathbf{T}}\mathbf{QR}\right]^{-1}\mathbf{R}^{\mathbf{T}}\mathbf{Q}^{\mathbf{T}}\right)\\ &= \mathrm{diag}\left(\mathbf{QQ}^{\mathbf{T}}\right)\end{aligned} \tag{11}$$

since $\mathbf{Q}^{\mathbf{T}}\mathbf{Q} = \mathbf{I}_{[p_i\times p_i]}$ and can be computed directly through the row norms $|\bar{Q}_j|$ of matrix $\mathbf{Q}$

$$\mathcal{K} = \mathrm{diag}\left(\mathbf{QQ}^{\mathbf{T}}\right) = \left[\,|\bar{Q}_1|^2,\ |\bar{Q}_2|^2,\ \ldots,\ |\bar{Q}_N|^2\,\right]^{\mathbf{T}}. \tag{12}$$

This last definition in (12) for the EI index is between 4 to 5 times faster than the classic formulation in equation (8) [21].

Concerning the notions of modal orthogonality and linear independence, they may be lost if the modal analysis procedures are indiscriminately used replacing the displacement mode shapes by the strain shapes, since the framework in modal analysis is generally based on the hypothesis that the displacement (or the acceleration) are the available output signals. In order to validate the latter instead, a theoretical derivation (for a FE model) was carried out by Yam *et al* [22], who showed that a strain mode is an energy equilibrium state as a displacement mode is, and therefore a modal parameter of the structure.

In an attempt to solve this problem, a transformation function between strain and displacement is suggested. This geometric transformation was detailed by Foss [23]: let us consider a FE model with r elements and m mode shapes. The strain matrix $\mathbf{s}$ and displacement matrix $\mathbf{d}$ can be expressed in modal coordinates $\bar{q}$ through the corresponding modal matrices $\boldsymbol{\Phi}_{\mathbf{s}}$ and $\boldsymbol{\Phi}_{\mathbf{d}}$:

$$\mathbf{s}_{[6\times r]} = \boldsymbol{\Phi}_{\mathbf{s}_{[6\times r\times m]}}\bar{q}_{[m]}, \tag{13}$$

$$\mathbf{d}_{[3\times r]} = \boldsymbol{\Phi}_{\mathbf{d}_{[3\times r\times m]}}\bar{q}_{[m]}. \tag{14}$$

Since in general $m \ll n$, a least-square approach leads to the determination of the modal coordinates $\bar{q}$:

$$\bar{q} = \boldsymbol{\Phi}_{\mathbf{s}}^{+}\mathbf{s} = \left[\boldsymbol{\Phi}_{\mathbf{s}}^{\mathbf{T}}\boldsymbol{\Phi}_{\mathbf{s}}\right]^{-1}\boldsymbol{\Phi}_{\mathbf{s}}^{\mathbf{T}}\mathbf{s}, \tag{15}$$

$$\mathbf{d} = \boldsymbol{\Phi}_{\mathbf{d}}\boldsymbol{\Phi}_{\mathbf{s}}^{+}\mathbf{s} = \mathbf{Ts}. \tag{16}$$

Theoretically, this linear transformation allows a direct safe-passage between modal strain analysis and modal displacement analysis. Experimentally, the results of modal reconstruction from strain and displacement data has been demonstrated to be equal [4, 22, 23] for flat specimens. Concerning the mathematical development, $\boldsymbol{\Phi}$ can be safely identified to either $\boldsymbol{\Phi}_{\mathbf{d}}$ or $\boldsymbol{\Phi}_{\mathbf{s}}$.

4.2. Placement optimization of PVDF transducers as actuators

Since the inverse energy transformation (electric to mechanical) is possible using the PVDF transducers, as shown in the literature [12, 28], it is possible to introduce actuation through PVDF film sensors. The optimization problem for actuators shares the same mathematical base as the equivalent problem in sensing. This means that for a given configuration of the PVDF network, all the modes that can be discerned can also be excited, and this is due to the symmetric relationship between mechanical and electric displacement in the fundamental piezoelectric equations [29]. If for example an EI-optimized PVDF network is considered, the transmission of the MKE is optimized for the whole set of considered modes. Those can be sensed and excited at the same time.

4.3. Manufacturing configuration

Each manufactured sample has a different configuration of integrated sensors network, based on optimization criteria as described in section 4.1. The number of minimum sensing transducers was fixed to three, for reasons further explained in [15] justified by a sensitivity analysis over the vibrational modes in the 0–2000 [Hz] band. This frequency range is wide enough to contain eight natural frequencies. Two optimized configurations were considered in the instrumentation of the samples.

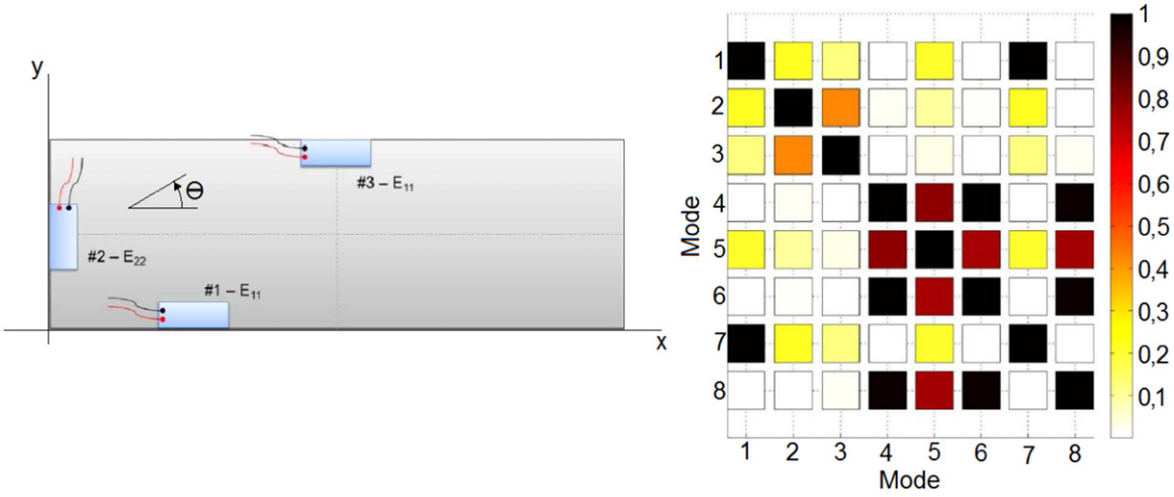

Figure 5. Configuration 1: $\mathcal{S}$-optimized placement, for 3 strain transducers.

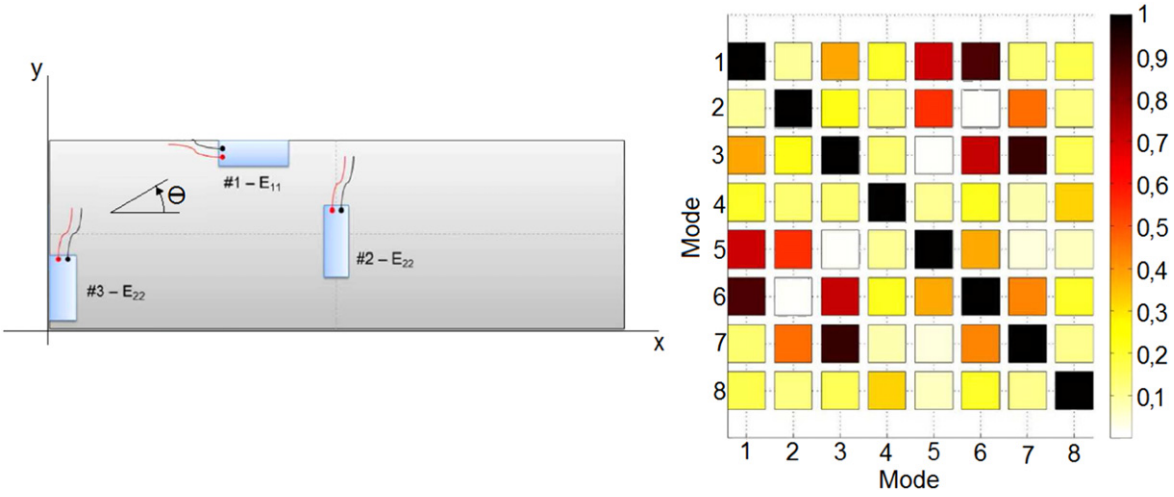

Figure 6. Configuration 2: $\mathcal{K}$-optimized placement, for 3 strain transducers.

(i) The naive method, which uses the principle of overlapping mode shapes to locate three regions where the whole set of 8 vibrational modes shows a deformation. Quantitatively, the optimization criterion is based on the values for vector $\mathcal{S}$, which is given by the following equation:

$$\mathcal{S} = \mathrm{diag}\left(\boldsymbol{\Phi}_{s,11}\boldsymbol{\Phi}_{s,11}^{\mathrm{T}} + \boldsymbol{\Phi}_{s,22}\boldsymbol{\Phi}_{s,22}^{\mathrm{T}}\right), \tag{17}$$

where $\mathcal{S}$ is a vector (similar to $\mathcal{K}$) of which each component represents the squared norm of the total strain of each sampling point in a FE model. $\boldsymbol{\Phi}_{s,11}$ and $\boldsymbol{\Phi}_{s,22}$ are $r \times m$ sub-matrices of the strain mode shape $\boldsymbol{\Phi}_s$ representing the longitudinal and transverse strains, for a given mode and at a given point. The three locations with the highest coefficients are taken into account. This approach is based on the Gram matrix theory.

(ii) A more sophisticated method, based on the EI technique and its result in equation (12), where the three locations with the highest coefficients in $\mathcal{K}$ are taken into account. The optimization process is detailed in the previous subsections.

Table 4. Location and orientation of PVDF patches in $\mathcal{S}$-optimized and $\mathcal{K}$-optimized configurations.

	$\mathcal{S}$-opt.			$\mathcal{K}$-opt.		
	x (mm)	y (mm)	θ (°)	x (mm)	y (mm)	θ (°)
1	75	2	0	112.5	98	0
2	2	50	−90	150	50	−90
3	150	98	0	2	25	−90

The corresponding computed optimal placements are shown graphically in figures 5 and 6 and in table 4, with the corresponding MAC analysis for the reduced FE model-based mode shapes. The locations are the coordinates of the PVDF patches middle points, and the orientations are expressed with respect to the longitudinal axes. As it can be seen, in the case of a CFRP plate with the nominal geometry 300 × 100 × 4.5 mm^3 and nominal elastic properties in table 2, three consecutive modes (4, 5 and 6) would eventually have some

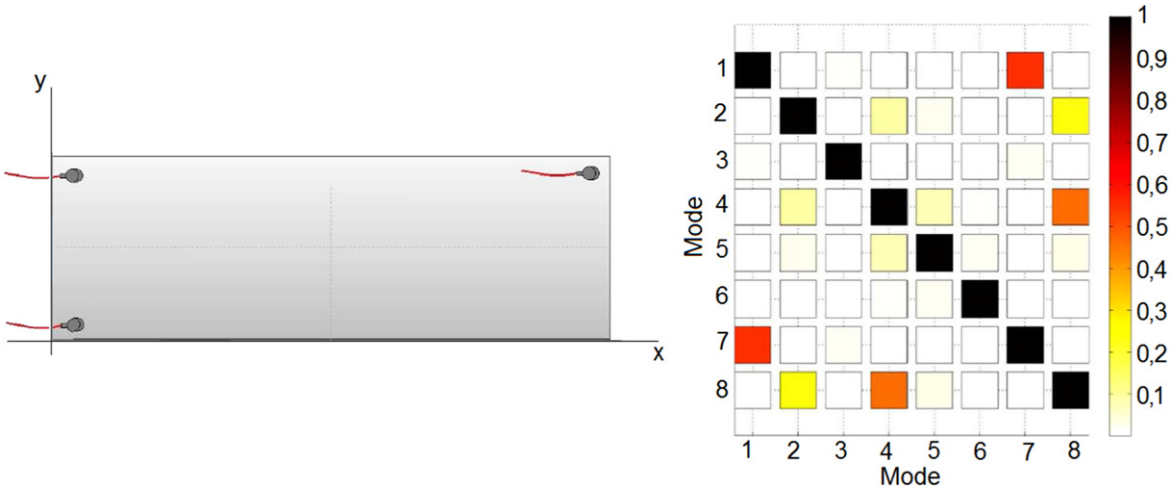

Figure 7. Optimal placement of a 3-accelerometer network.

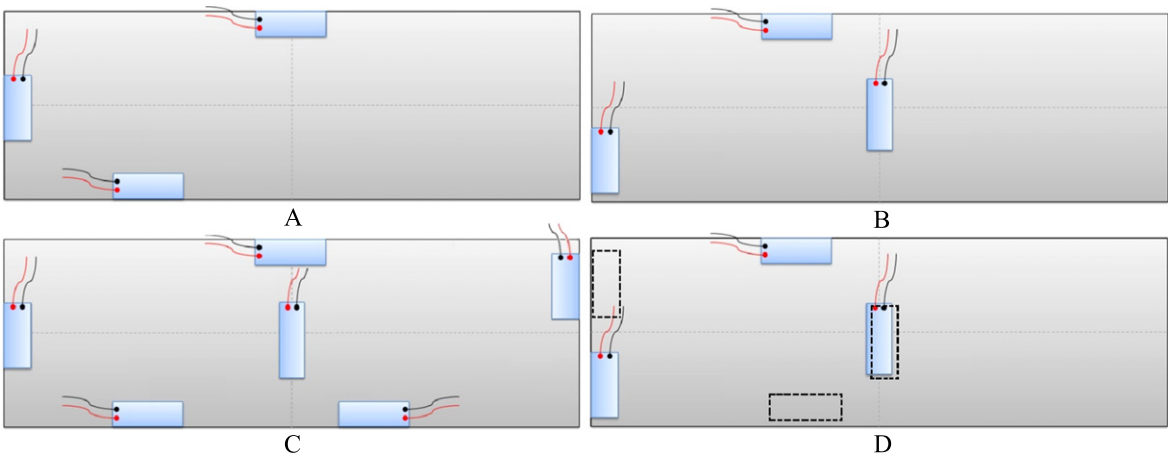

Figure 8. Transducer placement on the surface of the manufactured samples (a dotted rectangle symbolizes the transducer placement on the back).

modal extraction issues with the naive $\mathcal{S}$-based method, while these apparent issues are solved remarkably well with the EI $\mathcal{K}$-based method. Concerning a placement optimization based on displacement (or acceleration), both methods give indifferently as the optimal points the corners of the plate under free-free boundary conditions, as shown in figure 7. Placement diagrams for all test specimens are shown in figure 8. It should be noted that the MAC matrix for the accelerometers is more decoupled than the MAC matrix for PVDF sensors, which can be attributed to the non-orthonormality of strain mode shapes.

5. Experimental campaign

5.1. Planning

In order to carry out qualitative (visual inspection of SVD curves) and quantitative (error in the extracted natural frequencies) comparisons between standard (impact hammer, loud-speaker, accelerometers) and novel (fan, PVDF transducers) hardware for modal analysis, progressive evaluation of the OMA method have been tested. The experimental sequence is summarized in table 5, and the configuration for each specimen is given as:

Table 5. Test plan: EMA extracted natural frequencies are the reference, while OMA extracted natural frequencies are tested: IH = impact hammer, Sp = loud-speaker, Acc = accelerometer, PVDF = PVDF film transducers and fan.

Sample	Test	Actuator/sensor	Optimized configuration
A	EMA	IH/Acc	—
	OMA1	Sp/Acc	—
	OMA2	Fan/Acc	—
	OMA3	PVDF/Acc	$\mathcal{S}$-optimized
B	EMA	IH/Acc	—
	OMA1	Sp/PVDF	$\mathcal{K}$-optimized
	OMA2	Fan/PVDF	$\mathcal{K}$-optimized
C	EMA	IH/Acc	—
	OMA1	Fan/PVDF	$\mathcal{K}$-optimized
	OMA2	Fan/PVDF	$\mathcal{S}$-optimized
D	EMA	IH/Acc	—
	OMA1	PVDF/PVDF	$\mathcal{K}$-optimized
	OMA2	PVDF+fan/PVDF	$\mathcal{K}$-optimized

Table 6. Natural frequencies (in (Hz)) identified by an EMA, using an impact hammer and an accelerometer. Several measurements were carried out on each sample, in order to reduce the scattering (less than 0.1% of standard deviation for each mode).

Sample	1	2	3	4	5	6	7	8
A	237.1	397	600.7	1030.2	1059.1	1147.4	1261.4	1448.8
B	270.1	447.2	683.4	1162	1199	1322	1414	1677
C	247.1	409.2	630.4	1072.6	1097.2	1176.5	1342	1500
D	295.1	433	680.4	1148.2	1192.4	1246.2	1445	1631.6

Table 7. Summary table of the extracted natural frequencies from EMA and OMA, with the corresponding errors, with $\alpha = 5\%$ and $\nu = 7$.

Specimen	Test	$\bar{\epsilon}$ (%)	σ_ϵ(%)	$t = \frac{\bar{\epsilon}}{\sigma_\epsilon / \sqrt{n}}$	$t_{\text{crit}} = T_\alpha(\nu)$	Decision
A	OMA1	0.36	0.58	1.746	2.365	H_0
A	OMA2	0.05	0.36	0.375	2.365	H_0
A	OMA3	–0.63	1.51	1.183	2.365	H_0
B	OMA1	0.32	0.42	2.143	2.365	H_0
B	OMA2	–0.36	0.46	2.180	2.365	H_0
C	OMA1	–0.40	0.72	1.575	2.365	H_0
C	OMA2	–0.31	2.00	0.436	2.365	H_0
D	OMA1	0.31	0.78	1.103	2.365	H_0
D	OMA2	0.21	0.45	1.340	2.365	H_0

(i) Sample A using an $\mathcal{S}$-optimized configuration.
(ii) Sample B using a $\mathcal{K}$-optimized configuration (EI method).
(iii) Sample C using two configurations: an $\mathcal{S}$-optimized one and a $\mathcal{K}$-optimized one. The main idea is to compare and experimentally confirm the advantage of the latter over the former in discerning close mode shapes.
(iv) Sample D using a double $\mathcal{K}$-optimized network, for simultaneous actuation/sensing. The same configuration has been integrated on both faces.

6. Results

6.1. EMA results and identification

The extracted EMA frequencies are summarized in table 6. Those values are used as references to compare the quality of OMA.

In the following sections, a bias with respect to the EMA frequencies is defined as:

$$\bar{\epsilon} = \frac{1}{n^e}\sum_{i=1}^{n^e}\epsilon_i, \tag{18}$$

where $\epsilon_i = (f_{\text{OMA},i} - f_{\text{EMA},i})/f_{\text{EMA},i}$, $f_{\text{OMA},i}$ and $f_{\text{EMA},i}$ are the ith order extracted natural frequencies after an OMA or an EMA, and n^e is the number of extracted modes. The normalization is justified by the increasing value of the frequencies and in order to weigh correctly the measurement scattering. In table 7, a hypothesis test is carried out, where the null hypothesis H_0 is accepted if the bias is not statistically significant, and is rejected otherwise. The testing variable is defined by

$$t = \frac{|\bar{\epsilon}|}{\sigma_\epsilon/\sqrt{n^e}}, \tag{19}$$

where σ_ϵ is the estimated standard deviation of the bias, and $n^e = 8$. Under the null hypothesis, t follows a t-Student probability law $T(\nu)$, where $\nu = n^e - 1$ is the number of DoF. The critical threshold t_{crit} is evaluated with a significance level of $\alpha = 5\%$, and the null hypothesis is accepted if $t < t_{\text{crit}}$. As it can be seen in the last column of table 7, the global results are satisfying since the null hypothesis is accepted in all cases. Moreover, excepting two cases, the standard deviation σ_ϵ is lower than 1%, which points out a certain statistical coherence between the two methods.

These statements can be graphically verified by visual inspection of the SVD diagrams shown in figures 9–13. In these graphs, the vertical lines represent the EMA- and OMA-extracted natural frequencies, while the curves are respectively the first, second and third singular values contained in $\mathbf{S}_+(\omega_k)$.

6.2. Validation case: Sp/Acc and fan/Acc

A reference example (sample A) is set up in order to verify that the OMA algorithm implemented agrees with theory and the natural frequencies are correctly identified and to validate the use of a Intertronic 40CM stand fan as a white noise excitation source. Three accelerometers were deployed as in figure 7. The fan has a 40 cm diameter propeller, placed at 0.5 m in front of the specimen, turning at ∼1000 rpm. No harmonics are visible in the SVD spectra. The idea behind the use of a fan is the reduced scale similarity with the excitation of a plane in the turbulent airflow, a boat in a stream, or a race car on a track. However, its use should be validated by

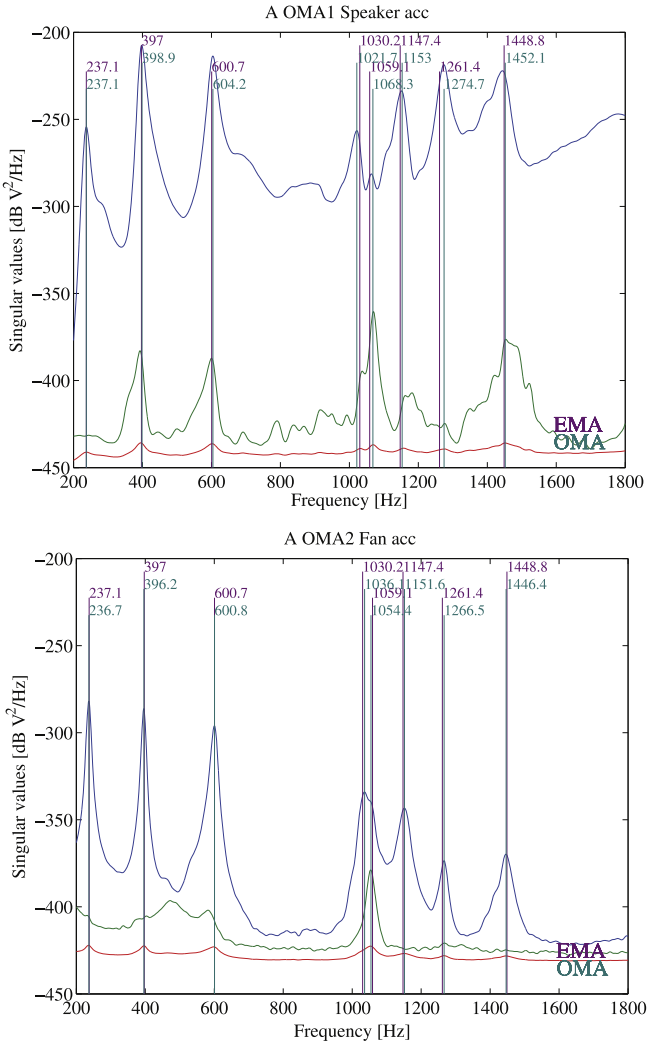

Figure 9. SVD plot for Sp/Acc and fan/Acc OMA combination.

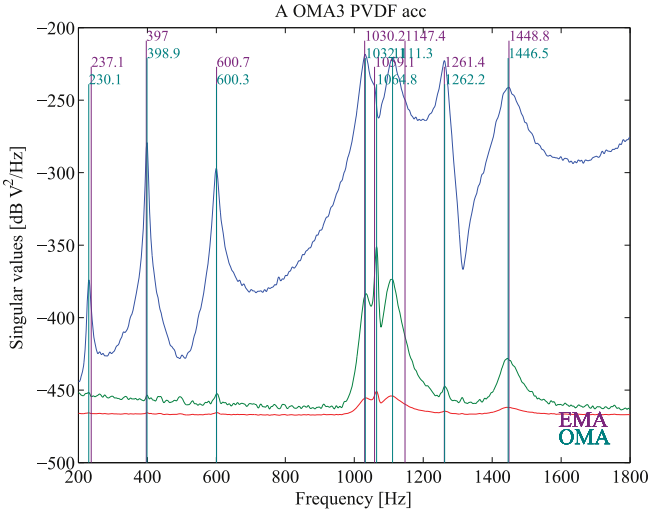

Figure 10. SVD plot for PVDF/accelerometers OMA combinations.

comparing the excitation of the fan with the excitation of a controlled actuator, which in this case is a loud-speaker. Thus, the randomness of the air flow and the excitation bandwidth

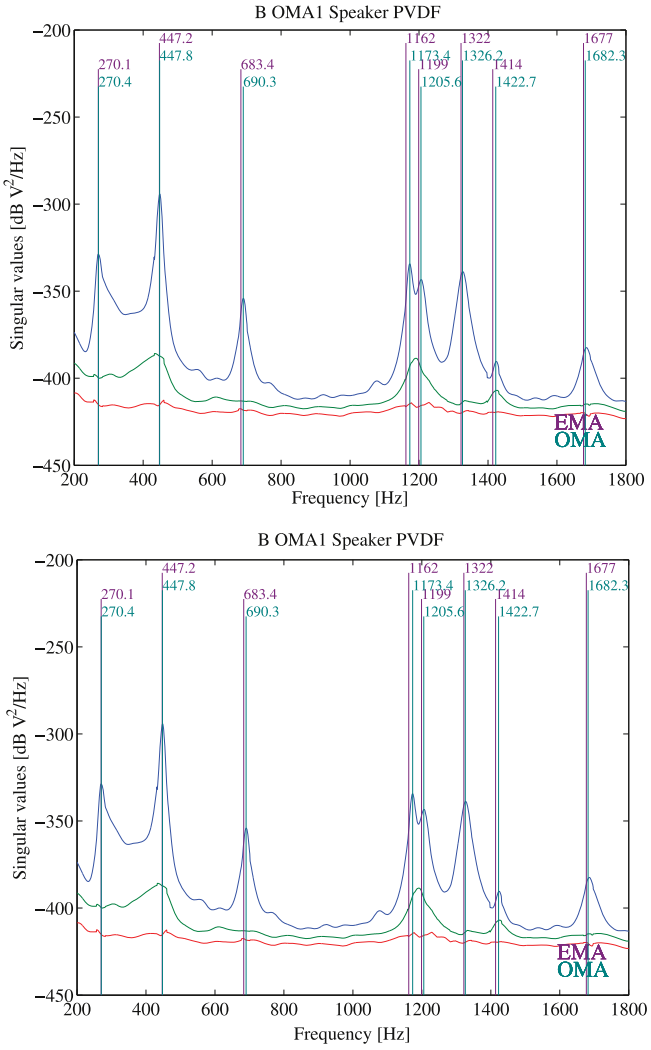

Figure 11. SVD plot for loud-speaker/PVDF and fan/PVDF OMA combinations.

of the fan can be compared to those of a frequency-controlled loud-speaker that provides a white-noise pressure field.

The quality of the graphs in figure 9 shows that the OMA has been well implemented as all resonance frequencies could be determined with moderate standard deviations. Since the frequencies are more accurate for the fan than for the loud-speaker, as shown in table 7 (which can be explained eventually by a higher delivered power), its use can be validated.

6.3. PVDF as actuators: PVDF/Acc

This constitutes the first series of OMA with PVDF patches as actuators, while three accelerometers were employed for sensing. As stated in the introduction, PVDF patches can theoretically excite the structure as strain actuators. As for the loud-speakers, a simulated white noise signal was used to excite each PVDF transducer individually (as mentioned before, gain is tuned at 100 and $V_{\text{peak}} = 500$ V in the SQV 1/500 piezo-amplifier).

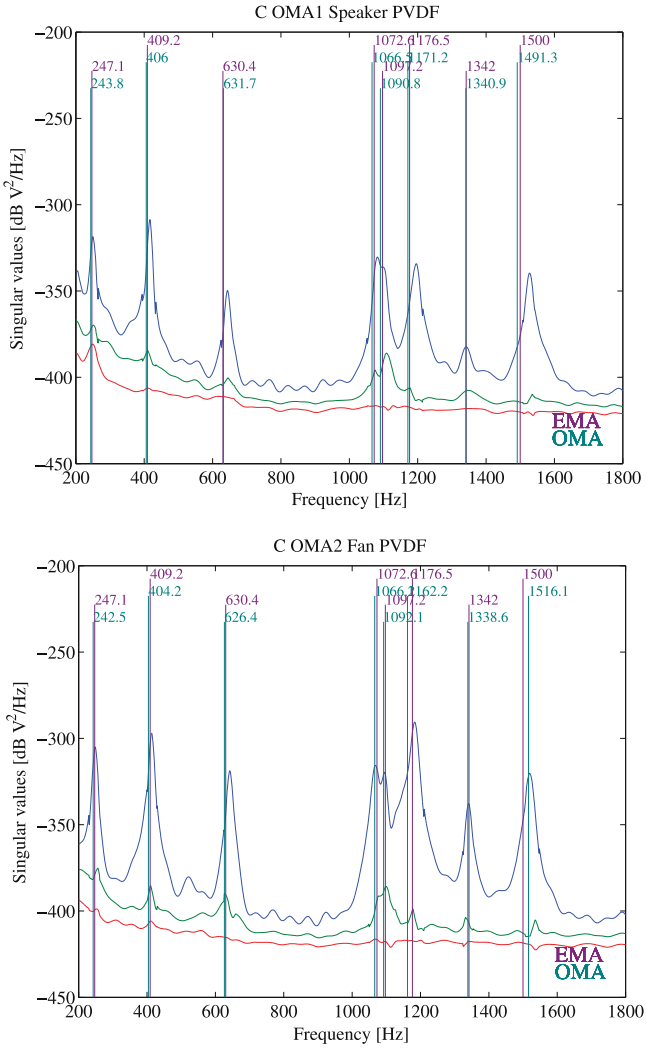

Figure 12. SVD plot for the fan/PVDF combination, test on two different configurations: $\mathcal{S}$-optimized and $\mathcal{K}$-optimized.

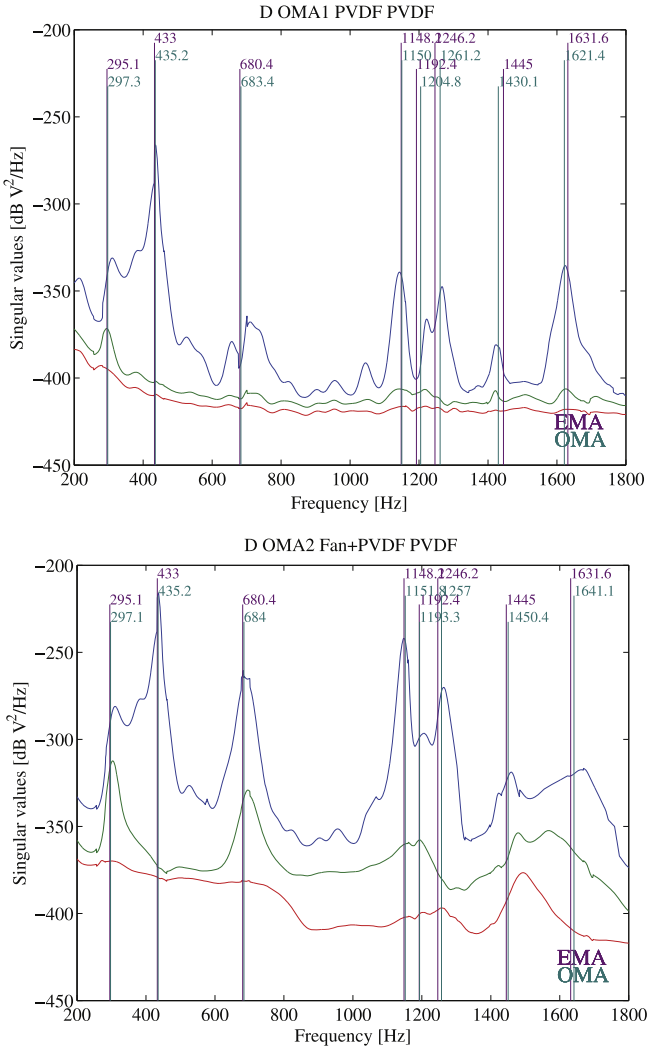

Figure 13. SVD plot for the PVDF/PVDF and fan+PVDF/PVDF OMA combinations, test with the $\mathcal{K}$-optimized network.

As it can be seen in figure 10, the PVDF patches work well as actuators, giving an accurate SVD plot. However, the modal extraction gives a standard deviation of 1.51% (table 7), which is higher than the experimental error given by the other combinations where accelerometers are the sensors. As it is investigated in the following sections, this is most probably due to the 'naive' placement of the PVDF sensors, since the network is $\mathcal{S}$-optimized rather than $\mathcal{K}$-optimized, and is then suboptimal for excitation.

6.4. PVDF as sensors: loud-speaker/PVDF and fan/PVDF

The second specimen (sample B) uses the PVDF transducers as sensors, with the $\mathcal{K}$-optimized placement for 8 modes. As for sample A, the center line of the fan and the loud-speaker were placed as close as possible in front of a corner in order to excite as many modes as possible. The main idea is to show if the PVDF transducer network can measure signals leading to a modal extraction as accurate as with an accelerometer network, using the OMA method.

As it can be seen in figure 11 and table 7, the standard deviation of the error is the same (about 0.45 %) for both excitations, and the same percentage as for the accelerometers networks (0.58% for Sp/Acc and 0.36% for fan/Acc). Optimally placed, PVDF transducers represent then an option as accurate as accelerometers.

6.5. PVDF as sensors: fan/PVDF in different configurations

The second feature to be explored is the comparison between the two optimization methods: based on the norm of strain modes or on the EI method, for what the sample C is analysed. The C OMA1 test is carried out with the PVDF network's $\mathcal{K}$-optimized configuration for sensing, while the C OMA2 test uses the $\mathcal{S}$-optimized one for actuation. The idea is to check the differences between these two methods, using the exact same sample.

Visually (figure 12),the quality of the SVD plots is the same. However, as it can be stated in table 7, the standard deviation is much higher in the case of the $\mathcal{S}$-optimized network (2.00%) than in the case of the $\mathcal{K}$-optimized one

(0.72%), making conclusive the improvement provided by the EI method.

6.6. PVDF as sensors/actuators: PVDF/PVDF

The experimentation with samples A, B and C has shown that PVDF actuation and sensing are possible. As a final stage of experimentation, it is logical to try one last sample equipped only with PVDF sensors and actuators. The fourth sample, named D, has two $\mathcal{K}$-optimized integrated networks of PVDF. As it can be seen in figure 13, the signal quality is satisfying.

The D OMA1 test shows an error level about 0.78%, slightly higher than the aforementioned results. The second test, D OMA 2, shows a supplementary test which combines PVDF transducers and fan excitation to achieve higher excitation. The inspiration for this test is based on the possibility to use both natural and artificial actuators (as it would be possible in full-scale structures and *in situ* tests): the natural excitation would be the principal source of energy, but in default of this, the PVDF complementary network would excite the structure to continue the OMA analysis. The final result shows a slight decrease of the error to 0.45%, for a PVDF excited band between 1000 and 2000 Hz.

6.7. Discussion of the results

According to the error percentages as summarized in table 7 for the whole set of OMA tests, the first statement about the scattering levels for the OMA tests involving PVDF patches is the consistency around approximatively the same values, included in the interval between 0.42% and 0.78%, with two notable exceptions: the A OMA3 test (PVDF/Acc, $\sigma_\epsilon = 1.5\%$) and the C OMA2 test (fan/PVDF, $\sigma_\epsilon = 2.0\%$). These last two tests have in common the involvement of a $\mathcal{S}$-optimized PVDF network in actuation/sensing, which could be associated with a lower performance with respect to $\mathcal{K}$-optimized PVDF network. Statistically, OMA and EMA can be considered statistically equivalent since the bias between both is proved insignificant. Concerning the usefulness of these measurements, the accuracy of the measured natural frequencies affects directly the accuracy of the material characterization, since these are related to the mechanical properties identification (by a factor of 2). Thus, the difference with respect to EMA would be in the 0.21–0.39% interval. As an example, the natural ageing of operational CFRP panels can approximately lead to a 10% loss of the local elastic properties. The accuracy of the technique suggested in this paper is in this case well adapted for a SHM application.

7. Conclusion

From the results stated in the previous section, several statements can be made. It has been demonstrated in this paper that the placement strategy proposed in [21], introducing the EI technique (with the strain mode shape modification), improves significantly the accuracy of the natural frequencies extraction from OMA.

As actuators, the PVDF transducers proved to be appropriate and suitable for SHM based on OMA, as long as they are optimally placed inside the composite structure. About the *a priori* concern about low stiffness, PVDF film transducers were capable of producing enough force to deform correctly a CFRP plate sample and provide enough power for the sensors to acquire. As sensors, PVDF provide remarkably accurate results with respect to accelerometers, confirming with this the results of previous papers by the authors [15, 25, 30]. Nevertheless, this needs to be verified in heavier structures in the future. The eventual association of PVDF actuation with a natural excitation source (in this case represented by a fan) shows to be a powerful complementary tool to natural excitation, and is strongly suggested to be explored further and used in SHM applications using OMA.

Acknowledgment

The authors would like to acknowledge the partial financial support from the Swiss National Science Foundation, Grant No. 200020-143968/1.

References

[1] Alvin K F, Robertson A N, Reich G W and Park K C 2003 Structural system identification: from reality to models *Comput. Struct.* **81** 1149–76
[2] Hurlebaus S and Gaul L 2006 Smart structures dynamics *Mech. Syst. Signal Process.* **20** 255–81
[3] Farrar C R, Doebling S W and Nix D A 2001 Vibration-based structural damage identification *Phil. Trans. R. Soc.* A **359** 131–49
[4] Ewins D J 2000 *Modal Testing: Theory, Practice and Application* 2nd edn (Hertfordshire: Research Studies Press Ltd)
[5] Tang L, Tao X and Choy C I 1999 Effectiveness and optimization of fibre Bragg grating sensor as embedded strain sensor *Smart Mater. Struct.* **8** 154–60
[6] Wood K, Brown T, Rogowski R and Jensen B 2000 Fiber optic sensors for health monitoring of morphing airframes: I. Bragg grating strain and temperature sensor *Smart Mater. Struct.* **9** 163–9
[7] Kister G, Ralph B and Fernando G F 2004 Damage detection in glass fibre-reinforced plastic composites using self-sensing e-glass fibres *Smart Mater. Struct.* **13** 1166–75
[8] Lynch J P and Loh K J 2006 Summary review of wireless sensors and sensor networks for structural health monitoring *Shock Vib. Dig.* **38** 91–128
[9] Mascarenas D, Todd M, Park G and Farrar C 2007 Development of an impedance-based wireless sensor node for structural health monitoring *Smart Mater. Struct.* **16** 2137–45
[10] Sze S M 1994 *Semiconductor Sensors* (New York: Wiley-Interscience)
[11] Liu C 2012 *Foundations of MEMS* (Englewood Cliffs, NJ: Prentice-Hall) Pearson International Edition
[12] Park G, Farrar C, Lanza di Scalea F and Coccia S 2006 Performance assessment and validation of piezoelectric active-sensors in structural health monitoring *Smart Mater. Struct.* **15** 1673–83

[13] Giurgiutiu V, Zagrai A and Bao J 2002 Embedded active sensors for *in situ* structural health monitoring of thin-wall structures *J. Press. Vessel Technol.* **124** 293–303
[14] Lin B and Giurgiutiu V 2005 Review of the *in situ* fabrication methods of piezoelectric wafer active sensor for sensing and actuation applications *Proc. SPIE* **5765** 1033–1044
[15] Guzman E, Cugnoni J, Gmür T, Bonhôte P and Schorderet A 2013 Survivability of integrated PVDF film sensors to accelerated ageing conditions in aeronautical/aerospace structures *Smart Mater. Struct.* **22** 065020
[16] Chen Z, Tan X, Will A and Ziel C 2007 A dynamic model for ionic polymermetal composite sensors *Smart Mater. Struct.* **16** 1477–88
[17] Wegener M, Schwerdtner R, Schueller M and Morschhauser A 2009 Dome-like pvdf actuators: preparation, phase transformation and piezoelectric properties *MRS Proc.* **1190** 1
[18] Jeon J H, Kang S P, Lee S and Oh I K 2009 Novel biomimetic actuator based on SPEEK and PVDF *Sensors Actuators* B **143** 357– 64
[19] Nestorović T and Trajkov M 2013 Optimal actuator and sensor placement based on balanced reduced models *Mech. Syst. Signal Process.* **36** 271–89
[20] Güney M and Eskinat E 2008 Optimal actuator and sensor placement in flexible structures using closed-loop criteria *J. Sound Vib.* **312** 210–33
[21] Li D S, Li H N and Fritzen C P 2007 The connection between effective independence and modal kinetic energy methods for sensor placements *J. Sound Vib.* **305** 945–55
[22] Yam L Y, Leung T P, Li D B and Xue K Z 1996 Theoretical and experimental study of modal strain analysis *J. Sound Vib.* **191** 251–60
[23] Foss G C and Haugse E D 1995 Using modal test results to develop strain to displacement transformations *Proc. SPIE* **2460** 112
[24] Zhang L, Wang T and Tamura Y 2010 A frequency-spatial domain decomposition (FSDD) method for operational modal analysis *Mech. Syst. Signal Process.* **24** 1227–39
[25] Guzman E, Cugnoni J and Gmür T 2014 Multi-factorial models of a carbon fibre/epoxy composite subjected to accelerated environmental ageing *Compos. Struct.* **111** 179–92
[26] Meo M and Zumpano G 2005 On the optimal sensor placement techniques for a bridge structure *Eng. Struct.* **27** 1488–97
[27] Kammer D C and Tinker M L 2004 Optimal placement of triaxial accelerometers for modal vibration tests *Mech. Syst. Signal Process.* **18** 29–41
[28] Giurgiutiu V 2008 *Structural Health Monitoring with Piezoelectric Wafer Active Sensors* 1st edn (Amsterdam: Elsevier)
[29] Tichý J, Erhart J, Kittinger E and Prívratská J 2010 *Fundamentals of Piezoelectric Sensorics: Mechanical, Dielectric, and Thermodynamical Properties of Piezoelectric Materials* (Berlin: Springer)
[30] Guzman E, Cugnoni J and Gmür T 2012 Accelerated isothermal and cyclic ageing of carbon fibre/epoxy composite panels with integrated PVDF sensors *ICEM15: Book of Abstracts 15th Int. Conf. Exp. Mech.* (*Porto, Portugal*) vol 7 pp 335–6